Geophys. J. Int. (1996) **126,** 147–165

Irregular grids in seismic tomography and minimum-time ray tracing

Aldo L. Vesnaver
Osservatorio Geofisico Sperimentale, PO Box 2011, 34016 *Trieste, Italy*

Accepted 1996 February 28. Received 1995 April 21; in original form 1994 September 12

SUMMARY

Tomographic inversion of traveltimes is often carried out by discretizing the Earth as a grid of regular pixels. This choice simplifies the related ray-tracing algorithms, but contributes significantly to the non-uniqueness of the estimated velocity distribution. A singular value decomposition of the tomographic matrix enables one to recognize the causes of this mathematical ambiguity in the model space. This is more intuitive than introducing arbitrary damping factors and spatial filters, and allows one to control the non-uniqueness of solutions by modifying the pixel distribution or the acquisition geometry. This approach lends itself to the adoption of irregular grids and to the definition of a new ray-tracing algorithm, based on Fermat's principle of minimum time, which is able to simulate transmitted, reflected, refracted and diffracted waves. The joint tomographic inversion of these different types of waves potentially provides an additional improvement to the quality and reliability of the estimated velocities.

Key words: inversion, ray tracing, tomography, traveltime.

INTRODUCTION

In the standard seismic processing for the exploration and production of hydrocarbons, the velocity analysis often relies on quite restrictive hypotheses, such as nearly horizontal reflectors and small incidence angles (Shah 1973; Al-Chalabi 1974, 1994). In this case, the traveltimes of the reflected arrivals at the surface may be approximated by the moveout curve, i.e. a function of the offset between source and receiver, the reflector depth and the sought velocity (Dix 1955; Taner & Koehler 1969; Hubral & Krey 1980). Recently, Boehm *et al.* (1996) compared the results obtained by the conventional stacking velocity analysis with those of reflection tomography. They showed that when the hypotheses of stacking velocity analysis break down, as in the presence of dipping reflectors or strong lateral velocity gradients, reflection tomography still provides accurate images of the geological structures.

Adopting more recent and general methods, such as the migration velocity scans (see for example the textbook by Yilmaz 1987), seismic waves with different propagation geometries (such as transmitted and reflected waves) cannot be jointly processed. Conversely, the traveltime inversion works better when sources and receivers are placed not only at the surface, but also in wells, and several type of waves (transmitted, reflected, refracted and diffracted) are picked. The images thus obtained are better resolved, and allow one to match data acquired with different geometries (such as VSP, cross-well and at the surface) and different frequencies (for example with sonic logs).

Tomographic estimation of local velocities by traveltime inversion is carried out iteratively, alternating two procedures: a forward modelling by ray tracing, and a back-propagation of the residuals (the differences between modelled and measured traveltimes). This procedure allows reconstruction of the depth model for the spatial distribution of velocities, which can significantly improve the quality of the depth migration. The main drawback of the linearized traveltime inversion is the non-uniqueness of its solutions, due to the so-called null space. Thus it may be necessary to treat the obtained results, and, therefore, their large-scale use, with some caution.

In this paper, I demonstrate that the null space can be reduced or eliminated by an improved design of the earth model. Some tools are introduced to measure the local reliability derived from the singular value decomposition of the tomographic matrix. This indicator can be used to merge adjacent pixels or to modify their boundary interactively, increasing the inversion stability and reliability.

The paper consists of two parts. In the first, an analysis of some of the causes of non-uniqueness in traveltime inversion solutions is carried out, which leads to the introduction of irregular pixels in the earth discretization. In the second part, a new ray-tracing algorithm is introduced, based on Fermat's principle of minimum time. This method allows a kinematic simulation of diffracted, refracted and converted waves, besides the more usual reflected and transmitted waves, in irregular grids.

THE INVERSION PROBLEM

In the popular approach to traveltime inversion, the Earth is modelled by pixels, i.e. zones where the local velocity (or its

gradient) is assumed to be constant. This simplification allows one to express the vector of measured traveltime vector **t** as a function of the unknown pixel slowness vector **u** by a linear equation

$$\mathbf{t} = \mathbf{A}\mathbf{u}, \tag{1}$$

where the element A_{ij} of the tomographic matrix **A** is the path length of the ith ray in the jth pixel. The problem is non-linear, since the ray trajectories depend on the unknown velocity values; it must be solved iteratively, therefore, alternately updating the velocity distribution and the ray paths.

The information carried by each ray to the inversion process is a row of matrix **A** in system (1). The transpose of this row can be considered as a vector associated with that ray. Two different rays may cross the same pixels in a particular grid, and sometime they may be associated with linearly dependent vectors. In some other space discretization, those rays may cross different group of pixels, so becoming certainly linearly independent.

Generally, matrix **A** is not square, and so I do not assume that the number of pixels equals that of rays. If we have fewer rays than pixels (and so fewer equations than unknowns), we know *a priori* that we have multiple solutions, but also in the opposite case, i.e. with more rays than pixels, we are not guaranteed that the system (1) has a unique solution. In fact, it is often the case that not all rows of the matrix **A** are linearly independent, so **A** may be rank-deficient anyway and a null space may exist. This means that vectors $\mathbf{u}_0$ exist which satisfy the homogeneous system

$$\mathbf{A}\mathbf{u}_0 = \mathbf{0}. \tag{2}$$

The null-space vectors cause the ambiguities in the traveltime inversion, since any vector $\mathbf{u}_0$ of the null space can be added to the solution of system (1) and a new solution obtained that fits the experimental data as well as the first one. We therefore obtain a space of solutions instead of a unique solution. Hence we must improve on this approach to finding the velocity distribution in the Earth from measured traveltimes.

DRAWBACKS OF SOME CONVENTIONAL APPROACHES

The most common solutions to eq. (1) adopt the least-squares criterion (see, for example, Claerbout 1976; Aki & Richards 1980; Lines & Treitel 1984), which provides more tractable equations. Unfortunately, the new equations system so obtained (for computer applications of practical interest) may be huge in two dimensions, and prohibitive in three dimensions. To improve the inversion stability and smoothness of the solutions, some damping term is often introduced. Usually, the damping parameter λ is found by trial and error (Levenberg 1944; Marquardt 1963). However, a subjective bias is thus introduced into the solution. It can also be demonstrated that the presence of a damping parameter significantly distorts the solution obtained (Lines & Treitel 1984). The resolution matrix **R** relates the estimated subsurface structure to the 'true' velocity structure (van der Sluis & van der Vorst 1987; Vasco 1991), and should be the identity matrix **I** if the inversion procedure is correct. By decomposing **A** and **R** into singular values (Golub & Van Loan 1983) in the case of a damped least-squares inversion, the singular values r_i of the resolution matrix **R** can be written as a function of the corresponding a_i of the tomographic matrix **A** (see Appendix A):

$$r_i = a_i^2/[a_i^2 + \lambda]. \tag{3}$$

For ill-posed problems, some values of a_i are very small or zero. We see from eq. (3) that, by increasing the damping factor λ, the denominator is moved away from zero but the singular values r_i are moved away from unity, so producing stable but distorted results. On the other hand, if we do not consider the coefficients not resolved by the data, our solution will remain largely undetermined.

Several other procedures have been introduced to stabilize the inversion at the expense of resolution: a comprehensive comparative review was carried out by Phillips & Fehler (1991). For example, local instabilities can be reduced by applying averaging or median filters, which smooth the velocity field, or alternatively the solution roughness can be limited by introducing into the object function some first- or second-difference operator.

SOME RECIPES FOR THE TRAVELTIME INVERSION

A good way to deal with the non-uniqueness of traveltime inversion is to reduce or even eliminate the null space. Two situations typically give rise to the null space:

(1) pixels not crossed by any ray;
(2) groups of two or more rays that are linearly dependent.

Both causes can be eliminated by modifying the tomographic grid. Fig. 1 shows (on the left) a conventional regular grid with a few straight rays and many void pixels, and (on the right) a possible modified grid, obtained by merging all void pixels with some neighbour crossed by at least one ray. We thus reduce the null space dimension, but the resolution decreases.

The fact that pixels not hit by any ray produce vectors of the null space is widely recognized, but this awareness has not led to adequate reactions. Void pixels could be simply ignored in the tomographic inversion, leading to the same algebraic result as by merging pixels. Nevertheless, zones with undefined velocity would appear in the model, and this fact is highly undesirable if the estimated velocity field has to be fed later to a ray-tracing procedure. This is, however, exactly what happens in the linearized inversion, where the ray paths and the velocity distribution are alternately updated. Furthermore, it is worthwhile to note that omitting the estimation of some pixel velocity is equivalent to adopting a regular grid with an irregular boundary: this is just half a step in the desired direction.

Pixel merging may be viewed as a nearest-neighbour interpolation. Naturally, higher-order interpolants or more sophisticated techniques based on stochastic constraints (see for example Neri *et al.* 1993) can provide results with a better apparent resolution. An effective resolution enhancement will be obtained, on the other hand, if and only if the actual velocity distribution has the same properties as the criterion chosen to assign the velocity in the void pixels, i.e. spatial smoothness for the higher-order interpolants, and some spatial texture for the stochastic constraints.

From the algebraic point of view, pixel merging corresponds to the summation of two adjacent columns of the tomographic

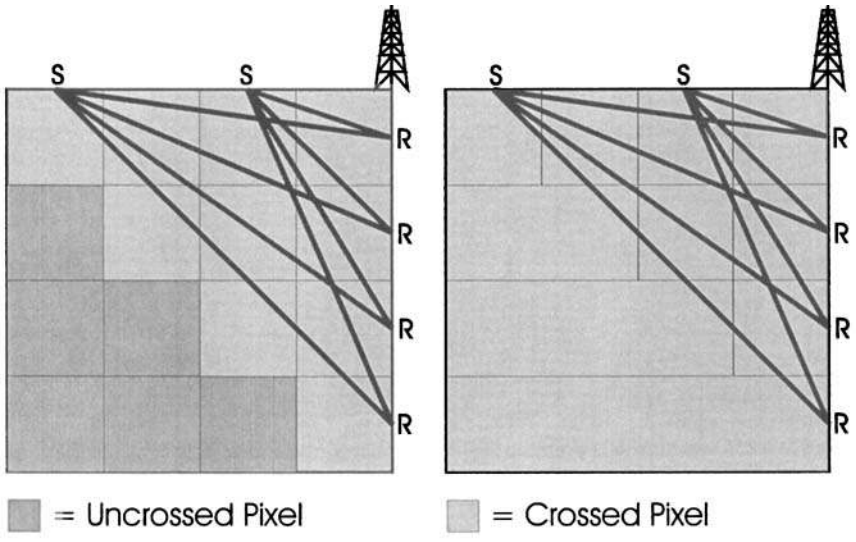

Figure 1. In a regular grid (left) with a walk-away VSP acquisition geometry, several pixels are not crossed by any ray, unlike in the irregular pixel discretization (right).

matrix, whose size is therefore reduced. Alternatively, the same effect is achieved by imposing the constraint that the velocities in the two pixels be the same:

$$u_i = u_{i+1}, \quad \text{or} \quad u_i = u_{i-1}. \tag{4}$$

This is nothing other than a hard constraint, which can be introduced very easily by an automatic computer program. The equation so added to the tomographic system reduces the uncontrolled degrees of freedom, but increases the computational effort. Therefore, the use of irregular grids should be preferred to the mathematically similar option of constraining.

In some cases the data can be better exploited by shifting the pixel boundaries without changing their total number. This operation can be carried out both to eliminate void pixels (Fig. 2) as well as to make two rays linearly independent (Fig. 3). (As the horizontal boundaries of pixels lie along parallel lines, Thales' theorem is valid: the initial segment of one ray is then proportional to that in the other ray, and this holds for all corresponding ray-segment couples.) In this way, 'global' resolution (the number of pixels) is not changed, but only the local resolution, in an attempt to obtain the best compromise between the desired resolution and the available rays.

Fig. 4 shows an example of two rays that are linearly dependent in a grid consisting of five pixels (left). If the lowest pixel is split into two parts, the rays become linearly independent (right), and their traveltimes can be explained to detect a possible lateral variations of velocity in the deeper zone.

As a conclusion to these considerations, the following empirical rules can be stated:

(1) merging adjacent pixels is a good way of removing uncrossed pixels, or zones poorly constrained by experimental data;

(2) shifting pixel boundaries may be an effective way to make rays that are not linearly independent into ones that are;

(3) splitting a pixel into two or more new ones allows a

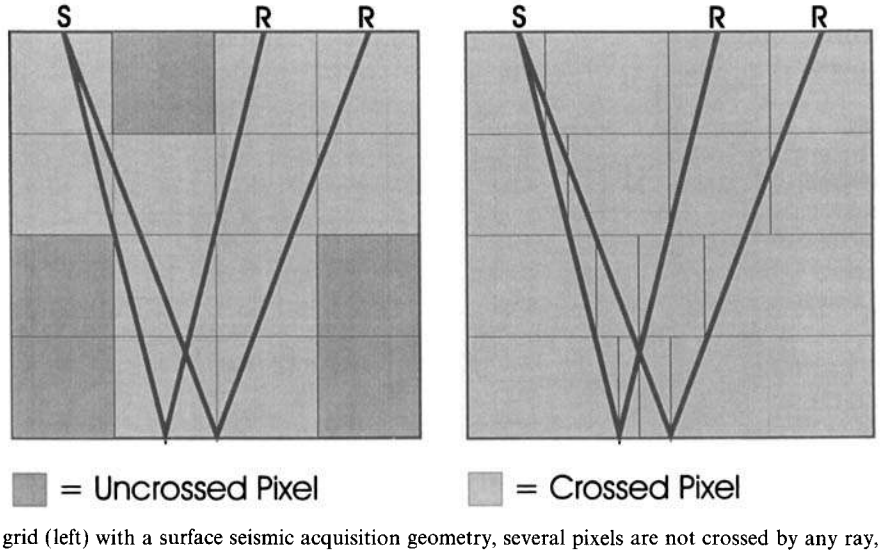

Figure 2. In a regular grid (left) with a surface seismic acquisition geometry, several pixels are not crossed by any ray, unlike in the irregular pixel discretization (right).

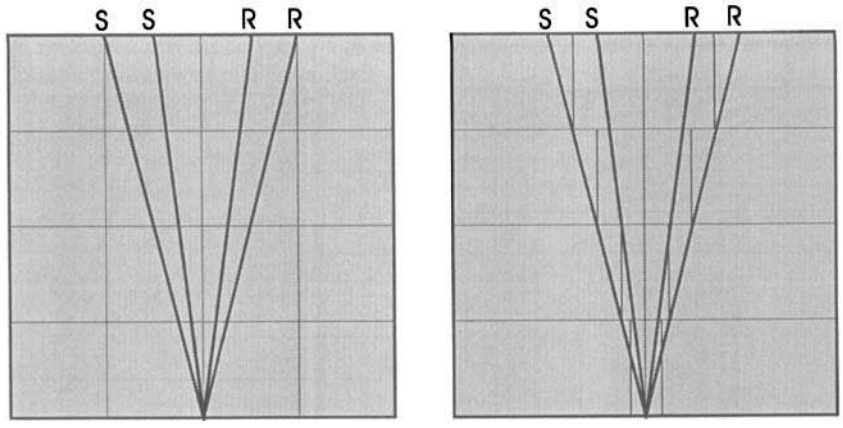

Figure 3. In a regular grid (left) with a common mid-point acquisition geometry, the two reflected rays are linearly dependent, but not in the irregular grid (right) obtained by shifting the pixel boundaries.

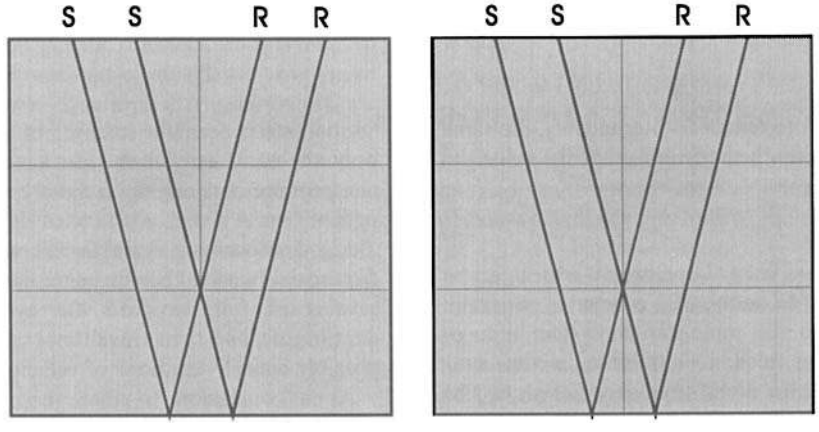

Figure 4. In a five-pixel grid (left) with a common mid-point acquisition geometry, two rays are linearly dependent, but not in the six-pixel grid (right) obtained by introducing an additional pixel boundary.

local increase in the resolution, provided that the new model discretization is sufficiently stable to support it;

(4) joining adjacent pixels will never make linearly dependent rays that cross each other become linearly independent.

Naturally, we need at least some quantitative hint to modify our model, especially when dealing with a large number of rays and pixels. In the next paragraph I will introduce an indicator for guiding an interactive application of these rules in practice.

The proposed approach is different from a method introduced by Bamford (1976): in that case, irregularly distributed sources and receivers are grouped into 'areas' to obtain a more robust parametric inversion of the velocity field, whose reliability is measured *a posteriori* by the traveltimes residuals and variance. Here, the solution reliability is estimated *a priori*, before its actual computation, by a singular value decomposition of the tomographic matrix.

THE USE OF SINGULAR VALUE DECOMPOSITION

Singular value decomposition of the tomographic matrix can be used to diagnose the possibility of inversion, and its stability. Singular values that are zero or too small with respect to the others cause serious difficulties and must be removed. The zeros can be viewed as the origin of the null space, whilst the very small values determine numerical instabilities, which can often produce data overflows or underflows.

I define the *quasi-zero singular values* as those that are smaller than a defined minimum threshold, which should be chosen taking into account the average of all singular values, as well as the available computer precision. The corresponding columns of the matrix **V** (defined in Appendix A) constitute an orthonormal basis of what could be called the *quasi-null space*, that is, the sum of the null space plus the ill-conditioned part of the range of matrix **A**.

A map of the quasi-null space is built in order to understand the inversion instabilities from a geometric point of view. The elements m_i of the vector map **m** can be defined as follows:

$$m_i = \sum V_{ij}^2, \tag{5}$$

where V_{ij} are the elements of matrix **V**, and the summation is carried out over the columns of the quasi-zero singular values only. Owing to the orthonormality of such basis vectors, values equal (or very close) to 1 will be obtained for some element m_i; the index of those equal to 1 will indicate pixels crossed by no rays or by very short rays.

What about linearly dependent rays? They can still be identified using the quasi-zero singular values by exclusion. In fact, once the quasi-void pixels are identified by the quasi-null space map **m** just described, the remaining quasi-zero singular

values will indicate the rows of the tomographic matrix **A** that are linearly dependent. So we identify the pixels that could be reshaped or split, getting more independent rays, and therefore reducing the null space dimension or increasing the local resolution respectively.

Fig. 5 shows a model composed of five layers over a half-space. Three shots with 48 receivers were simulated by the ray-tracing technique described below; the source interval is 500 m, and the receiver interval is 25 m. The first, third and fifth layers are homogeneous, with velocities of 1500, 2200 and 2700 m s^{-1}, respectively. In the second layer the velocity increases linearly from 1700 (left) to 2100 m s^{-1} (right); in the fourth layer the velocity ranges from 2500 (left) through 2100 (centre) to 2500 (right) m s^{-1}. The layer depths are (on the left) 200, 500, 750, 1050 and 1250 m, respectively.

Fig. 6 displays the estimated velocity and reliability (i.e. the vector **m**) obtained by the dual tomography algorithm (Carrion 1991). The practical implementation of this procedure is based on Kaczmarz's method, which does not require any damping factor (Kaczmarz 1937; van der Sluis & van der Vorst 1987). The same pixel discretization of the forward modelling was assumed for the inversion. A homogeneous medium with a velocity of 2200 m s^{-1} was the initial guess; this value remained unchanged in the pixels not crossed by any ray. The velocity field obtained (Fig. 6a) is reasonable but should be improved; the local reliability distribution (Fig. 6b) is lowest in the dark pixels, in particular in those uncrossed in the deeper part, and highest in the upper and central part. A certain instability may be noticed in both images in the first, third and fifth layers, which are homogeneous.

Merging all pixels in the first layer (Fig. 7) provides an important constraint (or *a priori* information) to the inversion process. The lateral gradient in the second layer is partially reconstructed, and also the velocity anomaly in the fourth (Fig. 7a). The estimated reliability is higher not only at the surface, but also in the whole central part (Fig. 7b).

A good result is obtained by merging the pixels in all the homogeneous layers (Fig. 8a): both the lateral gradient and the velocity anomaly are well resolved. The local reliability (Fig. 8b) is quite flat, except at borders (uncrossed pixels) and near the surface, where the coverage is much higher than in all other pixels.

THE GRID DESIGN

The proposed solution for reducing the null-space size actually introduces a new question: what is the best way to modify the pixel shape and distribution? This problem requires additional studies (see also Backus & Gilbert 1967; Vesnaver & Boehm 1995). Here I discuss some of the factors to be considered.

A viable practical solution is to use the singular values and the quasi-null-space vector map **m**. A flat reliability distribution should be sought interactively by merging, splitting or shifting the boundaries of adjacent pixels. Unfortunately, this problem is highly non-linear, since **m** depends on the ray distribution, and therefore also on the velocity field.

In the inversion examples just considered, I modified the lateral boundaries of pixels, assuming the reflectors' position to be known. This is a strong hypothesis, but it is quite realistic, if conventional surface seismic data are available, because reflection tomography can provide this information with a good accuracy (see, for example, Carrion *et al.* 1993a, b). Fig. 9 shows three velocity scans for the tomographic inversion of the seafloor in a seismic profile acquired by OGS in the Ross Sea (Antarctica). The optimal average velocity is 1460 m s^{-1}, because then the estimated reflection points (indicated by dots) are less dispersed: we can discern variations of only 0.3 per cent. Dots with different grey tones belong to different shots:

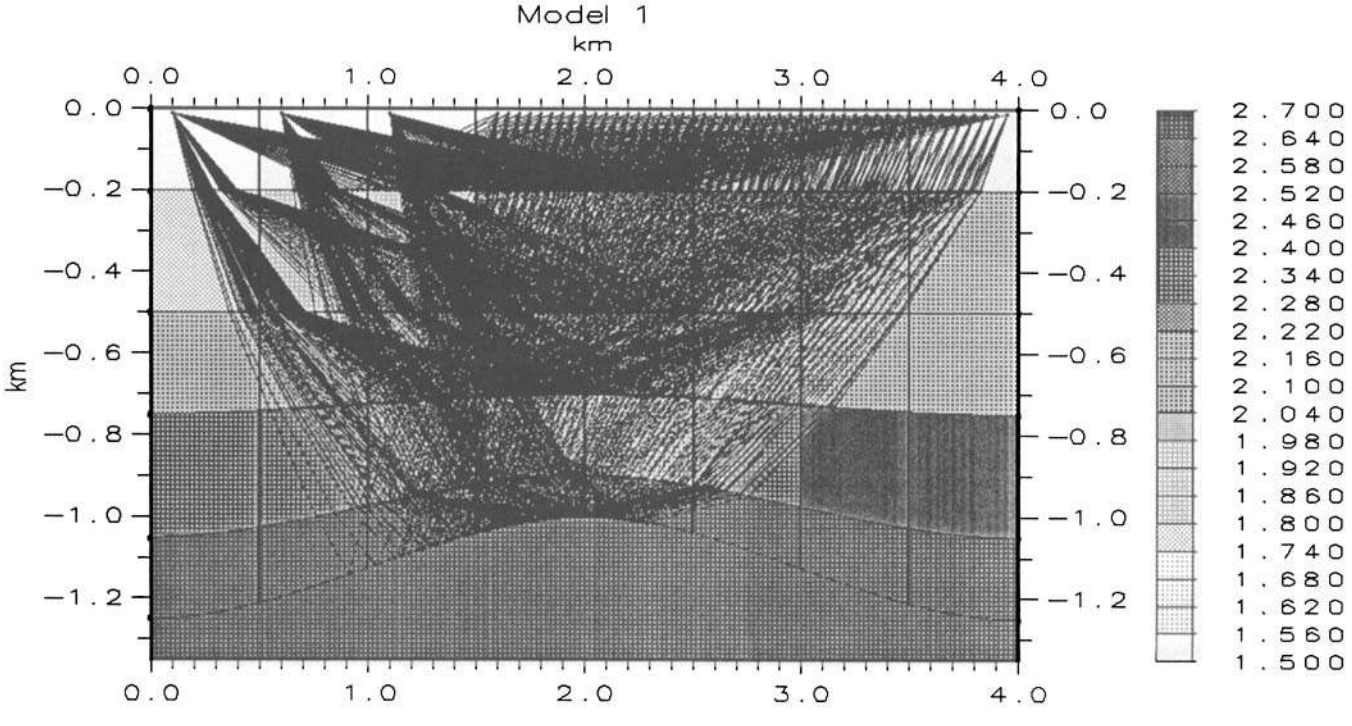

Figure 5. Model of an anticline with minimum-time ray paths.

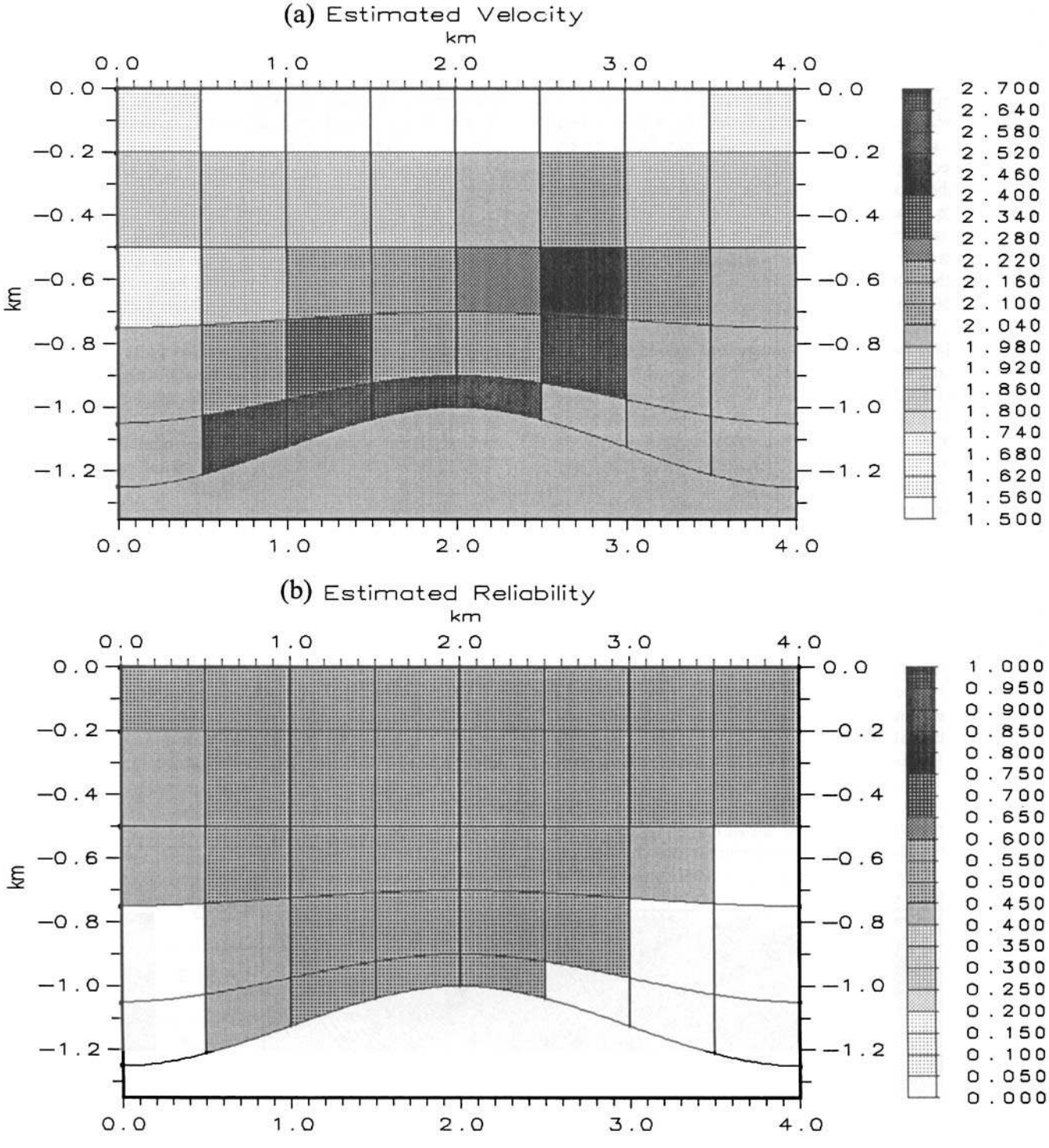

Figure 6. Estimated velocity (a) and reliability (b) with the same grid as the original model.

when the dispersion is minimum, the seafloor structure estimated by each shot is consistent with that of others. Another example of application to real data can be found in Boehm *et al.* (1995).

The pixel boundaries not associated with reflecting surfaces are much more questionable. Fig. 10 shows (top) a set of parallel rays crossing three pixels. The vertical boundaries can be shifted in several ways, without changing their partial traveltime: for example, by reducing the size and the velocity of the central pixels, or (leaving the velocities unchanged) by reducing the width of the first while increasing that of the third by the same amount, and so on. These degrees of freedom are reduced when the ray distribution better constrains the velocity distribution (bottom).

Some ambiguities may not be eliminated in the pixel design. If the rays and velocity distribution are uniquely determined, so are the intersection points of rays with the pixels boundaries; however, an infinite number of curves can be drawn that pass through these points (Fig. 11). This ambiguity decreases if many ray intersections are available around the pixels, and if

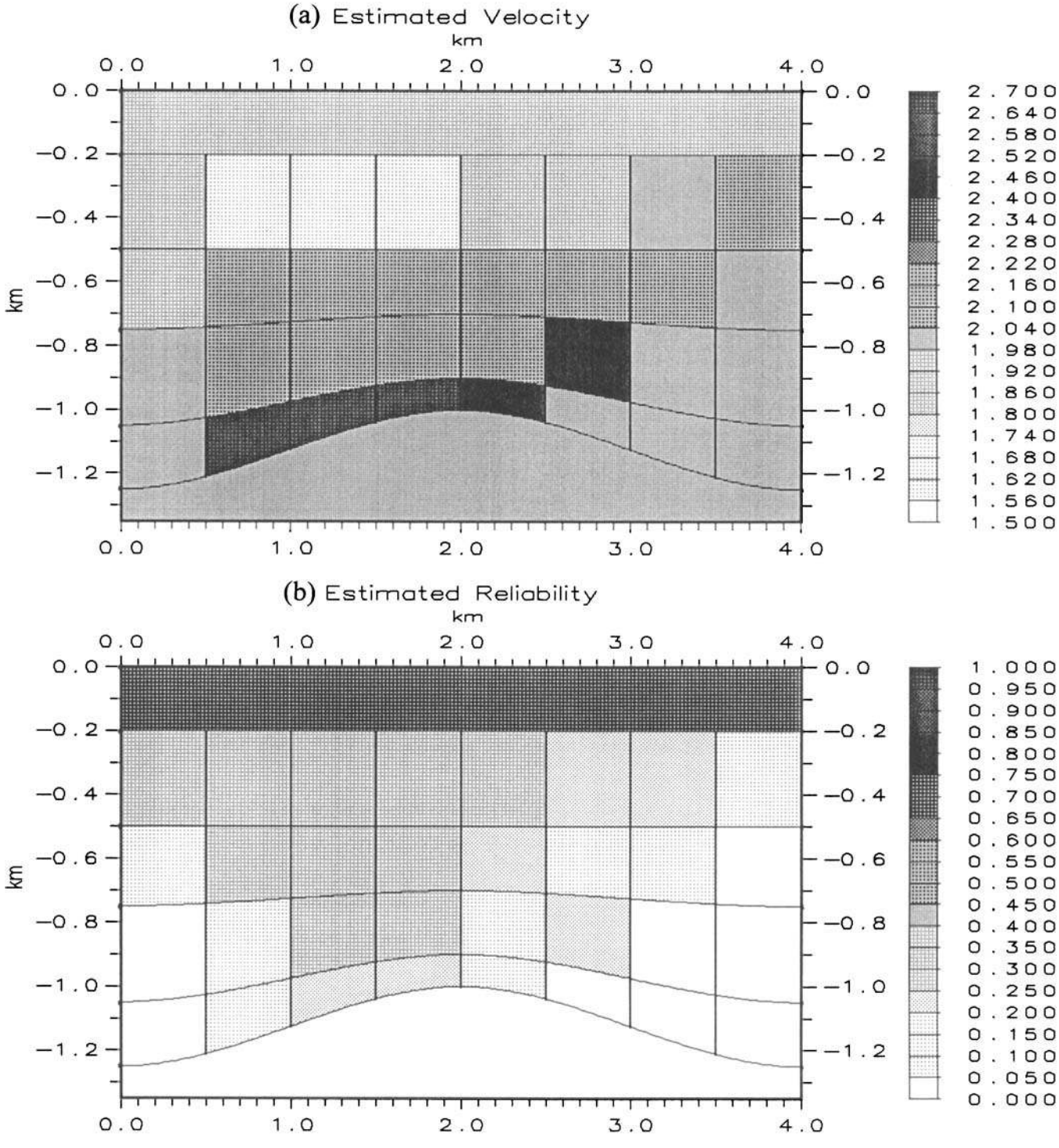

Figure 7. Estimated velocity (a) and reliability (b) after merging the pixels of the uppermost layer.

some class of smooth functions is chosen for the boundary definition. In this paper, vertical boundaries are described by straight lines and horizontal boundaries by splines.

ANGULAR COVERAGE IS NOT THE PROBLEM

Before concluding the first part of this paper, something should be said about the common conception that inversion instabilities and ambiguities are caused by an insufficient local angular coverage. This is certainly the case for reflected arrivals recorded at the surface, which are mostly near-vertical, but also in cross-hole acquisition geometry, where the seismic energy propagates mostly along nearly horizontal paths. Since these common seismic experiments in hydrocarbon exploration and production suffer from limited angular coverage of the target, this conception reflects adversely on tomographic methods: therefore many geophysicists think that tomographic

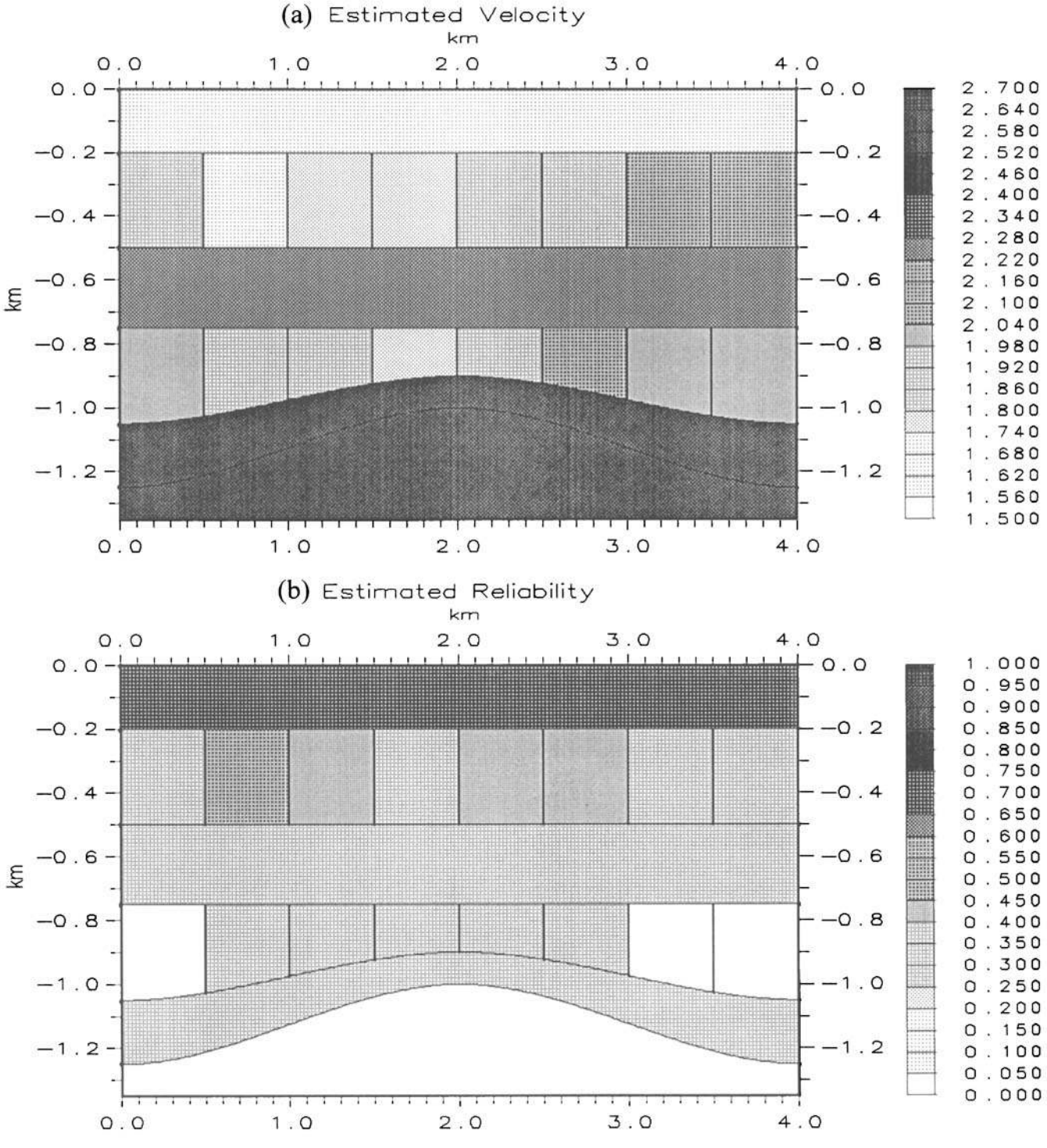

Figure 8. Estimated velocity (a) and reliability (b) after merging the pixels of the homogeneous layers.

inversion will never be sufficiently reliable. Let us consider this problem closely.

An insufficient local angular coverage may be an insuperable difficulty if the inversion problem is approached in continuous 2-D or 3-D space. Fortunately, there is clear evidence that this is not true when the space is discretized by pixels. Fig. 12 shows two common seismic experiments: well logging and well shooting. In both cases, the local angular aperture is practically zero; nevertheless, both methods are universally considered as very reliable for measuring seismic velocities. If the area penetrated by the wells is discretized as shown, the velocity field can be inverted without ambiguities: there is in fact a sufficient pixel *coverage*, and the ray paths are all linearly independent.

This idea is further explained in Fig. 13. The model is composed of two pixels only, which are crossed by rays with their sources located on the boundary of the first, and their receivers on that of the second, but not on the common

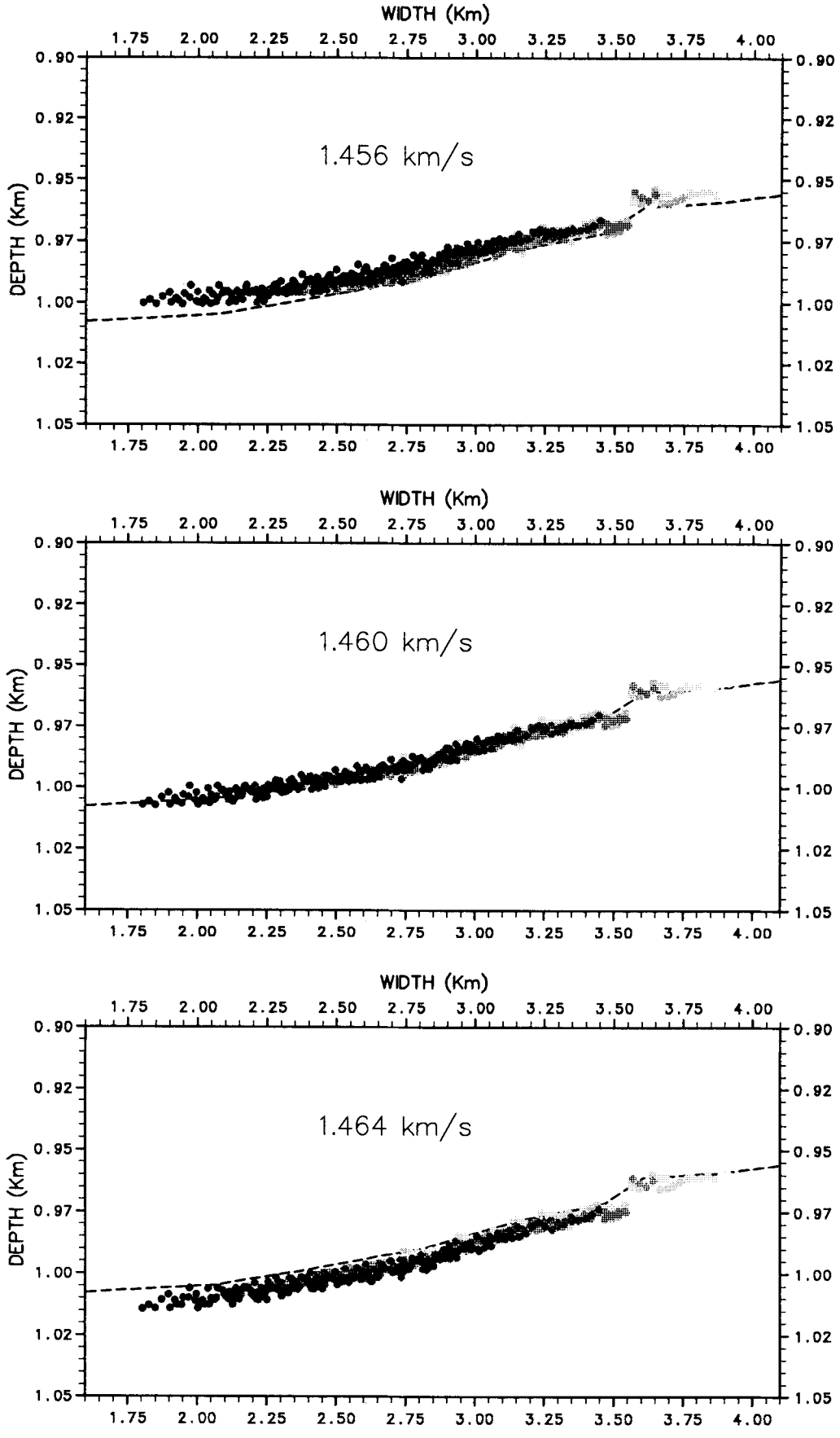

Figure 9. Tomographic inversion of reflected arrivals using three different average velocities between the sea surface and floor (see also Boehm *et al.* 1995).

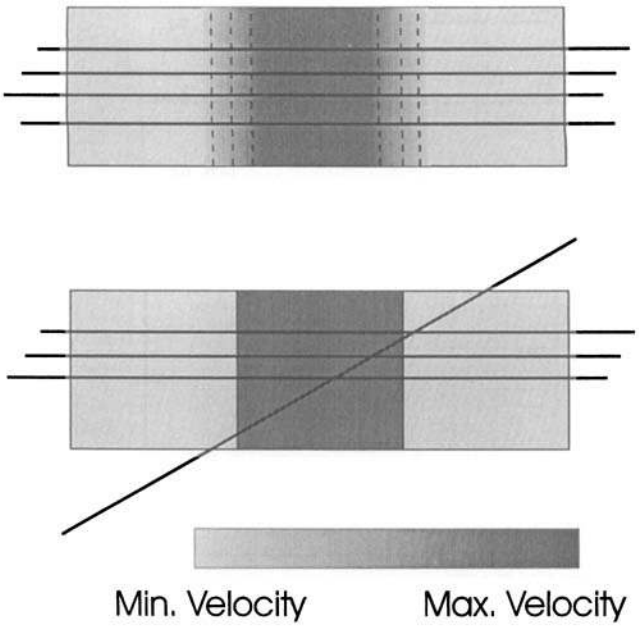

Figure 10. A set of parallel rays (top) does not sufficiently constrain the position of lateral pixel boundaries, unlike other configurations (bottom).

boundary. Let us suppose that the velocity contrast in the two pixels is small enough that straight lines may approximate the actual rays. Then, an infinite number of rays can be traced, covering the pixels at any angle, which are all linearly dependant. For example, this is shown for rays passing through the mid-point of the pixels' common boundary. This infinite number of rays, which provides a significant coverage of this simple model, does not provide a unique solution.

Another example is shown in Fig. 14. Let us assume that the velocity contrasts in the investigated medium are small enough to make ray bending negligible. In this case, we see that by simply rotating the pixels' orientation we can transform a tomographic inversion from undetermined (left) to well-conditioned (right). The model coverage of rays is the same in both cases, as is the pixel resolution. It should be emphasized therefore, that inversion feasibility depends on the relationship between all rays and all pixels.

Angular coverage is the false appearance of a real problem. If a set of rays are very close to each other, they may cross the same pixels; in this case, some of them may be (nearly) linearly dependent. If two or more rays cross different pixels, they are certainly linearly independent; this often happens when rays cross the same pixel at very different angles. Thus, when most pixels of the tomographic grid are crossed at various angles, it is reasonable to assume that the rows of the tomographic matrix associated with these rays are linearly independent, and so that the dimension of the null space is small or zero.

On the other hand, it was shown that introducing hard constraints gives similar results to increasing the angular coverage (Carrion *et al.* 1993c) or, in more precise terms, the model coverage: both operations reduce the influence of the null space.

THE USE OF DIFFERENT WAVE TYPES

P waves and *S* waves can be used to obtain two independent images of the velocity distribution in the Earth. A strong correlation can be expected between the two images, but, since the velocity ratio V_P/V_S is not constant, it cannot be used as a deterministic constraint: at the most it can guide an interactive model-driven interpretation. *P* and *S* waves can be properly related in the tomographic inversion if, in addition, converted waves are observed and picked.

A much more interesting role is played by refracted and diffracted waves, whose traveltimes can be directly compared with those of transmitted and reflected waves. The rays of refracted waves will generally cross some horizontally adjacent pixels along an interface, unlike reflected rays, and most of them will be linearly independent of the reflected rays: therefore, they will provide new information for the tomographic inversion, reducing the dimension of the null space. Similarly, the ray paths of diffracted waves are useful for reconstructing the velocity distribution around the diffraction points; here several rays branch at different angles according to geometries that are quite different with respect to those of reflected, transmitted and refracted waves, and therefore will be mostly linearly independent. This usually undesired type of wave should be exploited, therefore, as a local increase in information that improves the tomographic image of fault edges. This philosphy is not new to the analysts processing seismic profiles: seismic migration collapses the energy diffracted by faults to image their edges, while at the same time refining the migration velocities.

MINIMUM-TIME RAY TRACING

As a provisional conclusion to the first part of this paper, I note that a method for reducing the null-space dimension (and

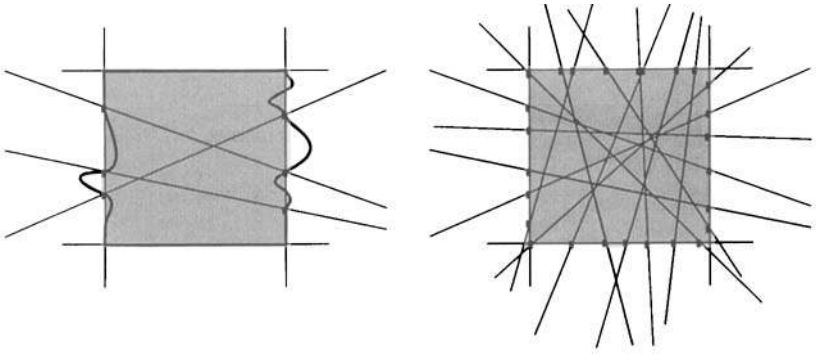

Figure 11. Several curves may intersect the rays at the same points (left), but this ambiguity can be reduced if more intersections are available (right).

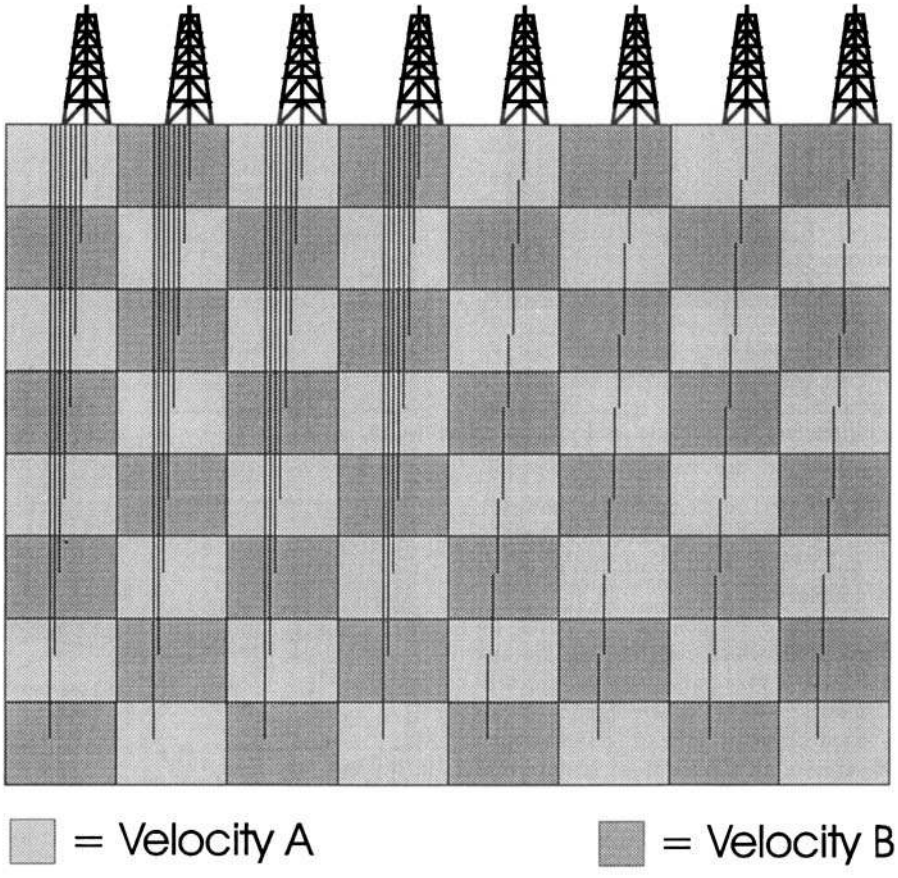

Figure 12. Well-shooting (left) and sonic-log (right) experiments can provide a perfect model reconstruction with a null angular aperture.

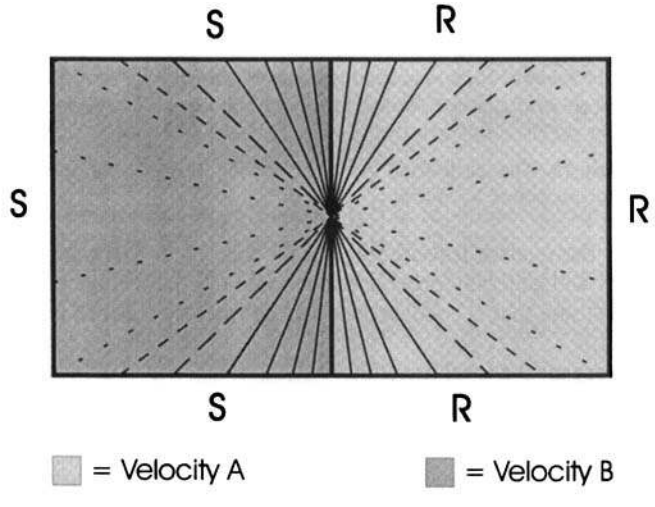

Figure 13. A simple model of two pixels can be covered by an infinite number of rays with full angular coverage, which are all linearly dependent.

the related indefiniteness of the tomographic inversion) is to discretize the Earth by irregular pixels, designed or iteratively fitted to the available rays to make them as linearly independent as possible. Second, not only transmitted or reflected, but also refracted and diffracted P waves should be simulated by the ray-tracing algorithm, in order to exploit their independent information with respect to the other wave types. Finally, if one intends to carry out a joint inversion of P and S waves, converted waves should also be generated; otherwise, in fact, P and S ray segments are the coefficients of uncoupled tomographic equations, with uncoupled estimation of V_P and V_S velocities.

Conventional techniques fail to produce all the types of waves together. Rays can be computed by finite-difference methods based on the wave equation; this approach allows computation of the amplitude of the propagating wave, and not just its traveltime and ray path (see among others: Julian & Gubbins 1977; Nolet 1987; Cerveny 1987; Vidale 1988, 1990; Virieux & Farra 1991; Pereyra 1992; Zelt & Schmidt 1992). On the other hand, numerical instabilities may occur in some of these algorithms if strong inhomogeneities or strongly dipping layers are present; in other cases, it is not possible to derive the velocity field at pixels boundaries. Thus, some other approach to ray tracing was sought, for these reasons as well as to reduce the required computational effort (and sometimes also the required computer memory).

An alternative solution relies on the minimum-time principle of Fermat. Some recent papers have introduced fast and stable algorithms of this type, which seem very amenable to the tomographic inversion of traveltime. Moser (1989, 1991), Saito (1989) and Fischer & Lees (1993) proposed some shortest-path ray-tracing techniques, discretizing the spatial distribution of velocities by regular networks: the ray is computed by minimizing the traveltime from the source to the receiver, and passing through the network nodes. Asakawa & Kanawaka (1993) suggested a way to eliminate the approximations due to network quantization by interpolating the traveltimes between

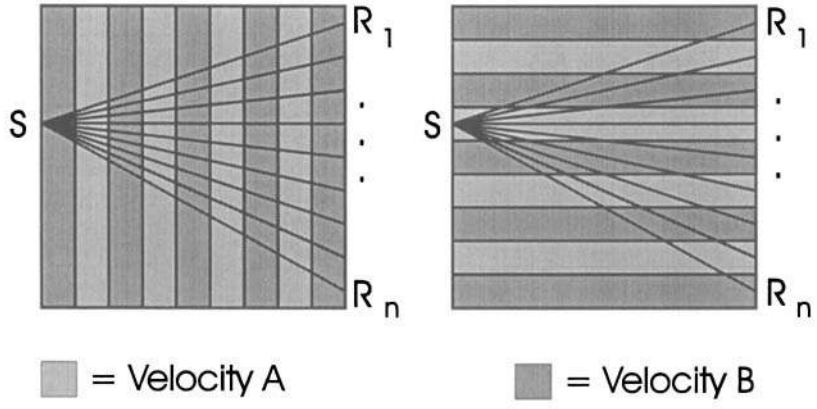

Figure 14. The same ray distribution is not able to resolve the model on the left, but is sufficient for that on the right.

the network nodes. Their practical implementation, however, still requires a noticeable regularity in the node distribution, and involves overheads due to the initial computation of the traveltimes along many couples of nodes.

In the following paragraphs, a further method based on Fermat's principle is introduced, which does not require any regular network. In particular, a very parsimonious representation of the velocity field is possible where homogeneous zones are assumed; for example, sea water can be represented by a single pixel. At the same time, a local fine discretization can be introduced into the target zone or where lateral variations are present. Similarly, the reflecting interfaces can be defined by a few points only, facilitating user interaction with the reflection tomography algorithms.

THE RAY-TRACING ALGORITHM

Since the propagation velocity is assumed constant inside each pixel, the ray path is a line composed of straight segments, determined by the intersection points of the ray with the pixel boundaries. For assigned source and receiver positions, the ray path can be computed as the piecewise linear path connecting them with the minimum traveltime for a seismic signal. The key point of the algorithm is that Fermat's principle can be applied not only to the whole ray, determined in general by several points, but also to its parts. In particular, any triplet of consecutive points along the ray path must satisfy Fermat's principle.

The iterative minimization procedure can be started with an initial guess, which can even be very rough: for example, a straight line from the source to the receiver (for transmitted waves), or a straight line from the source to a point in the reflecting interface and then from there to the receiver (for reflected waves). The initial guess determines what is sometimes called the ray signature.

In general, the traveltime along the initial guess will not be a minimum. The traveltime along the whole path can be decreased by reducing that in all the triplets of consecutive points. Let us consider three adjacent points A, X_0 and B (Fig. 15). The traveltime t_0 from A to B measured through the central point X_0 can be compared with t_1 and t_2 obtained from the perturbed ray points X_1 and X_2, respectively, located along the pixel boundaries. A new point can thus be calculated to substitute for X_0 in the triplet, and a parabola passing through the points (x_i, t_i), given by the abscissae of the ray points X_i,

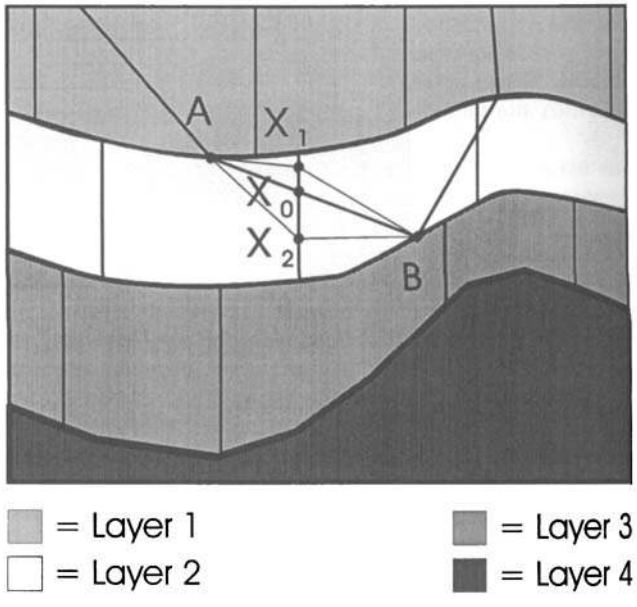

Figure 15. The path from A to B passing through X_0 and the perturbed points X_1 and X_2.

and the relative traveltimes, can be computed. The parabola apex will generally provide the abscissa of a new point with a traveltime that is smaller than for the three considered points (x_i, t_i).

Very often a local traveltime reduction in a triplet of adjacent points is achieved by such a parabolic fit, but not always. When it is not, the point just computed with abscissa x_4 and partial traveltime t_4 can be used to build a fourth-order rational function (see Appendix B). If its minimum x_5 still does not provide a traveltime smaller than all preceding estimates, it is possible to go on increasing the order of the rational function. It is only rarely that orders higher than the sixth are needed.

The traveltime minimization in the triplets can be carried out using various strategies. The considered triplet can be moved forwards along the path from the source to the receiver (as implemented here); or forwards and backwards, proceeding from source or receiver towards the ray centre and vice versa (Fig. 16). The second strategy is more amenable to parallel implementations, and is more consistent with the reciprocity principle. The iterations required are generally not many, and

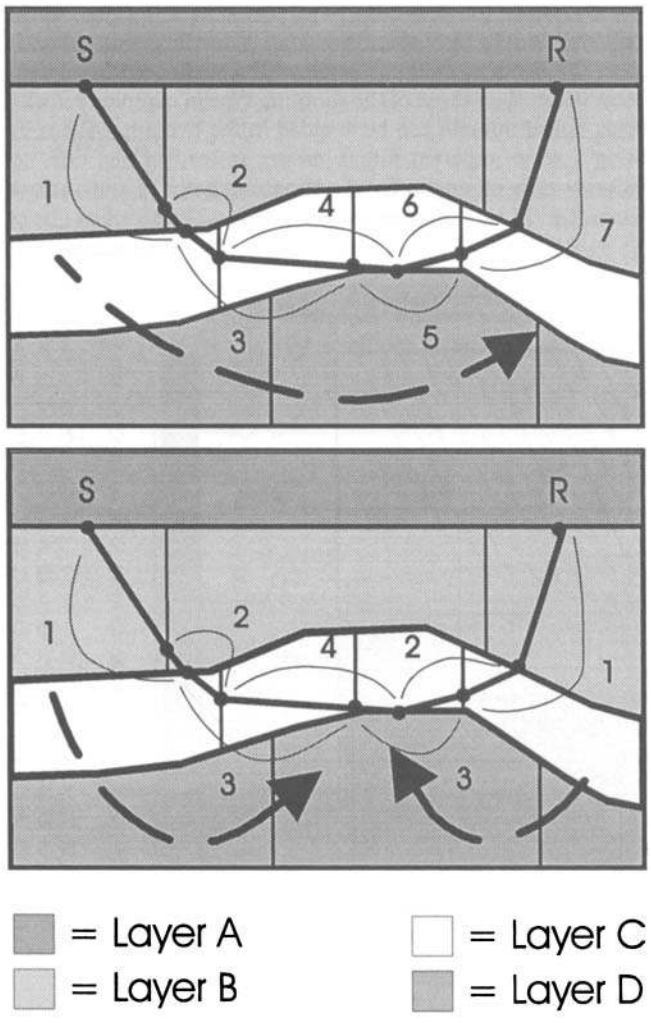

Figure 16. The minimization procedure can proceed from left to right (above) or can be split into two parts (below), starting from the source and the receiver and proceeding towards the centre of the ray path.

may be stopped when the sum of the ray-point variations is smaller than a predetermined threshold. Some comparison tests carried out with simple models have demonstrated that the proposed algorithm provides results with the same precision in a shorter time with respect to finite-difference solutions.

In the actual algorithm implementation, long pixels were chosen whose lateral boundaries are vertical lines, whilst the upper and lower boundaries coincide with tracts of the reflecting horizons. This choice was due to the fact that the ray-tracing code was designed to be part of a reflection tomography program. Since vertical velocity gradients cannot be reconstructed very well by conventional surface seismic data (see, for example, Carrion *et al.* 1993a), they are not taken into account.

The precision of ray-tracing algorithms is quite hard to estimate or compare: in fact, some methods require smooth velocity variations and others do not. If full-waveform modelling is assumed as a reference, the problem of picking the traveltime of seismic signals arises, with difficulties due to interfering waves, time sampling, possible phase rotations, and so on. In a few cases, an analytic solution is available, such as for a single homogeneous layer with parallel interfaces. I simulated a shot with 100 receivers, spaced 25 m apart, over a reflector with a depth of 1 km and a velocity of 1500 m s^{-1}, discretizing the illuminated space by an increasing number of pixels. The traveltime at each receiver was correct typically to the first five significant digits. The precision depended on the model discretization (Fig. 17): a plot of the logarithm of the sum of absolute traveltime errors versus the pixel number shows a nearly linear trend.

The convergence rate of the proposed algorithm decreases when the number of pixels is very large, and so I introduced some tricks to speed up the minimization convergence. First of all, Snell's law provides an analytical solution to the traveltime minimization in the triplets, except when diffractions occur. Although Snell's law would be in any case automatically 'discovered' by the procedure itself, some iterations are spared. Second, I exploited the information about the medium's behaviour carried by the neighbouring rays that have just been computed. By translating and stretching the shape of these known rays, a good initial guess and consequently a much faster convergence towards a minimum-time condition can be obtained.

Some intelligent strategy has to be adopted to relate the ray points to the pixels. In fact, this operation is trivial in regular grids, but may be quite time-consuming in irregular ones. A consistent speed-up was obtained, for example by storing the pointers to the pixels crossed by the previous ray (or previous iteration in the minimization procedure for that ray). If common source, common receiver or common mid-point gathers are simulated, the pointers to the corresponding ray parts will not change a lot, and I used the previous pointers to initialize the search for the new one required. It is not necessary to have a lot of memory for this: it is sufficient to store the last pixels crossed in the down-going and up-going parts of the ray path for each model layer.

The computer code implementing the proposed method is composed of some thousands of instructions. A significant number of them are used for moving the ray nodes around the boundaries of the irregular pixels. Fortunately, this boring work pays off: the pixel edges may behave as diffractors, therefore producing waves that cannot be simulated by adopting Snell's Law only or smooth velocity fields.

As for all minimization problems, the search for the path with a minimum traveltime is impeded by local minima. From the ray's point of view, local minima correspond to multiple paths for a given source–receiver configuration. This case is quite common, for example when a seismic profile passes

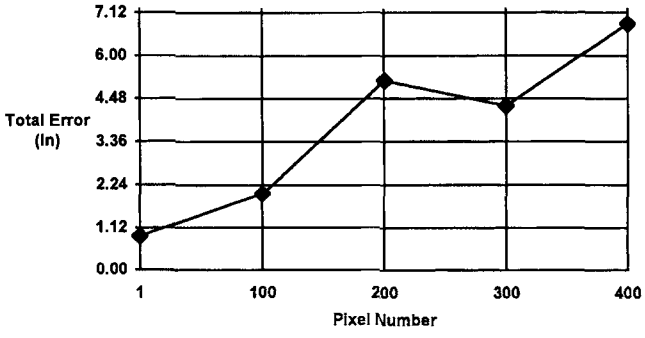

Figure 17. The logarithm of the total traveltime error versus the pixel number in a model with a plane parallel layer.

above a syncline. A classic pathological example is to place the source and receiver at the foci of an elliptical reflector, so that each reflecting point corresponds to a minimum-time path. In these cases, the final solution depends strongly on the initial guess.

The minimization may fail, providing a local minimum, when both strong and sharp velocity anomalies are present and the initial guess is far from the true solution, but works very well in relatively smooth media. According to my experience, the bending methods (such as that proposed here) converge better than those of the shooting type in complex velocity fields. Local minima can be avoided in the two approaches by using a set of different initial guesses instead of just one, i.e. different take-off angles for the shooting methods and various

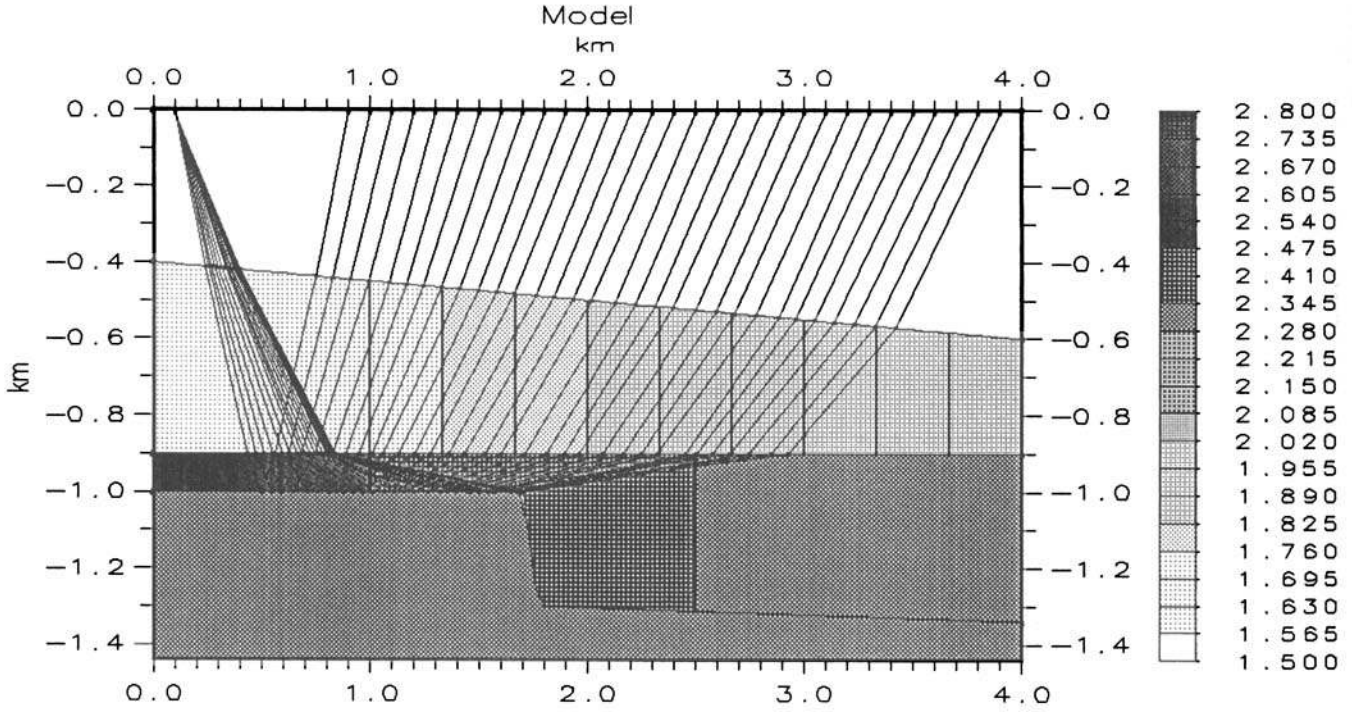

Figure 18. A model with a fault step and a laterally increasing velocity in the second layer. Diffracted rays can be observed.

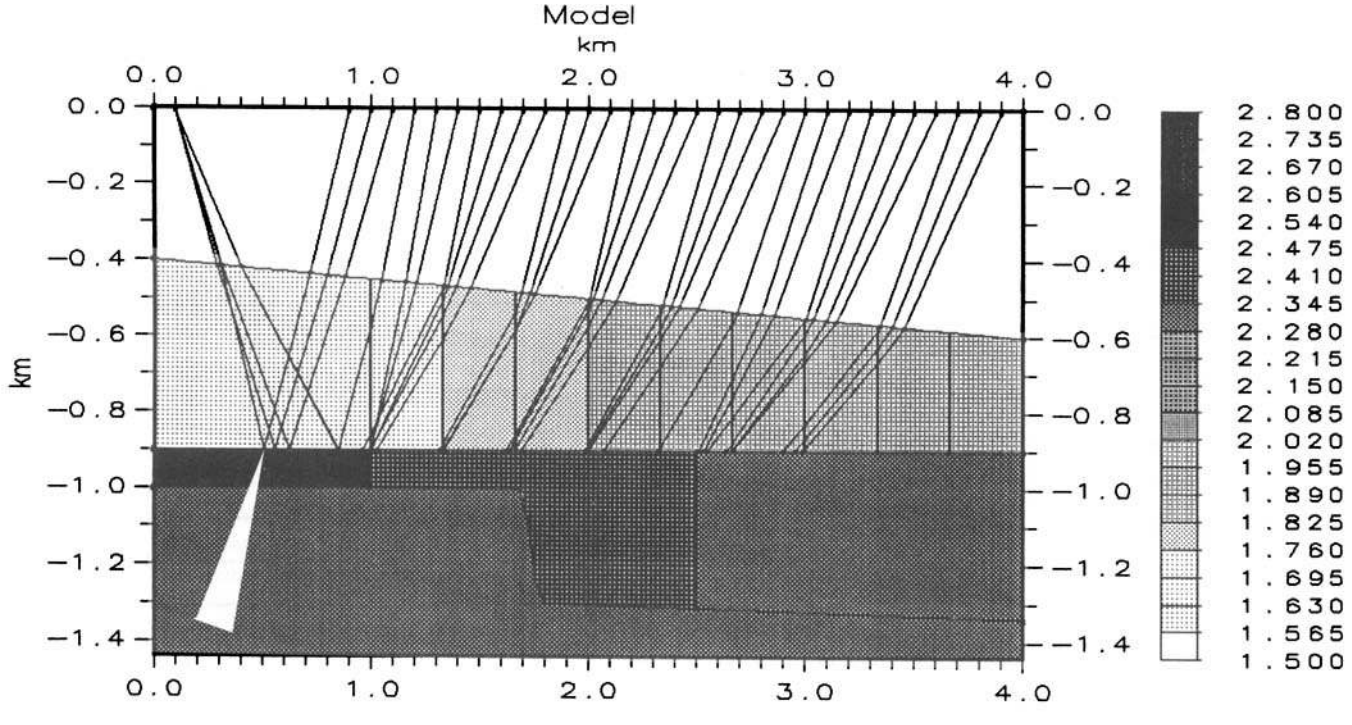

Figure 19. Rays of refracted waves in a flat model. The arrow indicates a collapsed couple of points, indicating that the offset between source and receiver is smaller than the critical distance.

initial paths for the bending methods. If distinct solutions are obtained, we can choose the ray path associated with the first arrival only or consider all of them.

EXAMPLES

Fig. 18 shows a model with a fault edge in a laterally varying velocity distribution: the rays corresponding to diffracted arrivals can be clearly seen.

Fig. 19 shows a nearly flat model, where the paths of refracted waves were computed. To obtain refracted waves instead of reflected ones, it is only necessary to insert two or more points lying on the chosen marker instead of only one. Naturally, if the velocity distribution and the interface geometry are complex, it will not be known if the offset is larger than the critical distance. If the distance between source and receiver is smaller than the critical distance, these two (or more) points along the marker will collapse into a single point,

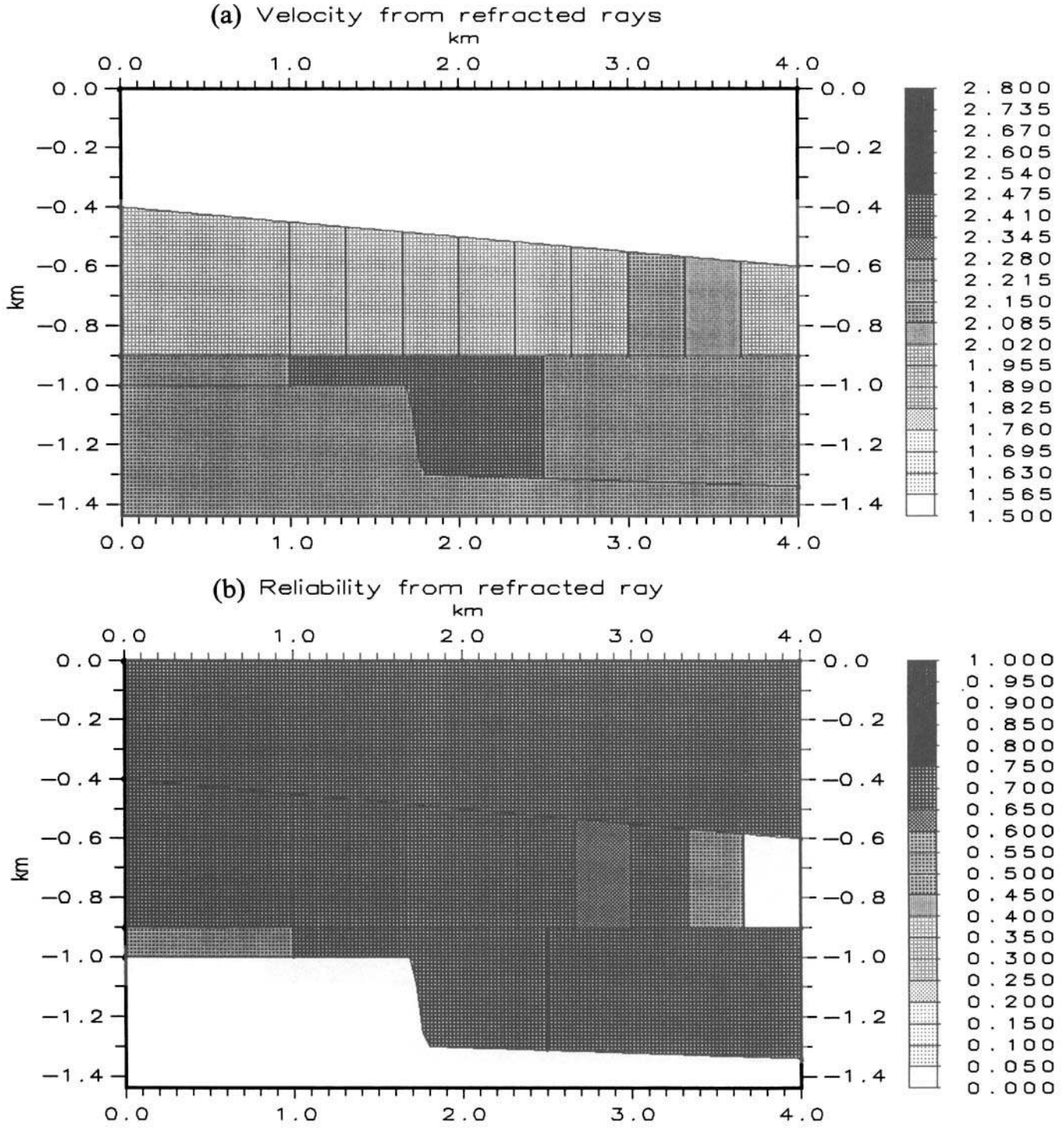

Figure 20. Estimated velocity (a) and reliability (b) of the model in Fig. 19, using refracted waves.

and a simple reflected wave is obtained: this is the case for the four leftmost rays in the figure. The nature of the wave is therefore guessed initially to be refracted, and this is confirmed, or not, at the end of the traveltime minimization.

This 'automatic' feature of the algorithm can be exploited to compute the critical distance at any depth for arbitrary geological structures. Starting with an offset close to zero, it is possible to trace rays initially assumed to be refracted waves, increasing the offset gradually: the smallest offset such that the refracted part of the ray path does not collapse into a single point will be the critical distance sought. In Fig. 19 this condition is satisfied close to the fourth ray from the left. In general, two different values for it are expected, by moving the receiver either left or right away from the source.

Fig. 20 displays the estimated velocity and reliability obtained by inverting the refracted arrivals. The reconstruction of the lateral gradient is good not only in the layer just above the refractor, but also below it. A poorer result is obtained by reflected ray paths (Fig. 21): the velocity gradient in the second layer was revealed but with some incorrect oscillations, and the underlying layer (not crossed by the reflected rays) was not determined. Comparing the two reliabilities (Figs 20b and 22b), we notice that a flatter distribution characterizes the estimate by refracted waves; this result is consistent with that of the previous inversion example, where we obtained better results by adapting the pixel distribution and flattening the reliability field.

Converted waves can be simulated very easily, using the P or S propagation velocity for the ray-path segments crossing the chosen domains or layers (Fig. 23). In the most general case, for each pixel it is necessary to define both V_P and V_S velocities. A mode conversion at an interface is simulated by switching from one velocity type to the other when the ray crosses an interface. Thus, an increase in the required computer memory can occur, but this is not always the case: in fact, if the velocity types along the ray are symmetric (e.g. *PSPPPSP*, as in Fig. 23b), it would be possible to store only the proper velocity values (V_P or V_S) for each layer.

CONCLUSIONS

The null space of the tomographic matrix is the cause of the non-uniqueness of solutions in the linearized inversion of traveltimes. If we extend its definition, a quasi-null space can be introduced which is also responsible for the numerical instabilities. Limited angular coverage is not an obstacle to a successful inversion, but only an empirical indication of possible rank deficiency in the tomographic matrix, which has to be verified using singular value decomposition.

The dimension of the (quasi-) null space can be reduced or zeroed by adopting a simple trick, such as eliminating uncrossed pixels or trying to obtain linearly independent rays by moving the pixel boundaries. In this way, we transform a rank-deficient system into an overdetermined one. The solution so obtained is unique in the mathematical sense, is more robust with respect to noise (such as mispicks of traveltimes), and does not require any initial model nor any *a priori* information about the velocity distribution to guide the algorithm.

As a consequence of this inversion procedure, we have to deal with irregular grids, whose local resolution depends strongly on the acquisition geometry and the spatial distribution of seismic velocities. In other words, we have to adapt our model to the available data. The local reliability, estimated by a singular value analysis, is a practical tool for an interactive grid optimization.

An important advantage of irregular grids is the possibility of reducing the pixel density in zones that are nearly homogeneous (such as sea water) or do not affect the target: here, on the contrary, the resolution can be maximized according to the available data and desired reliability. This flexibility is

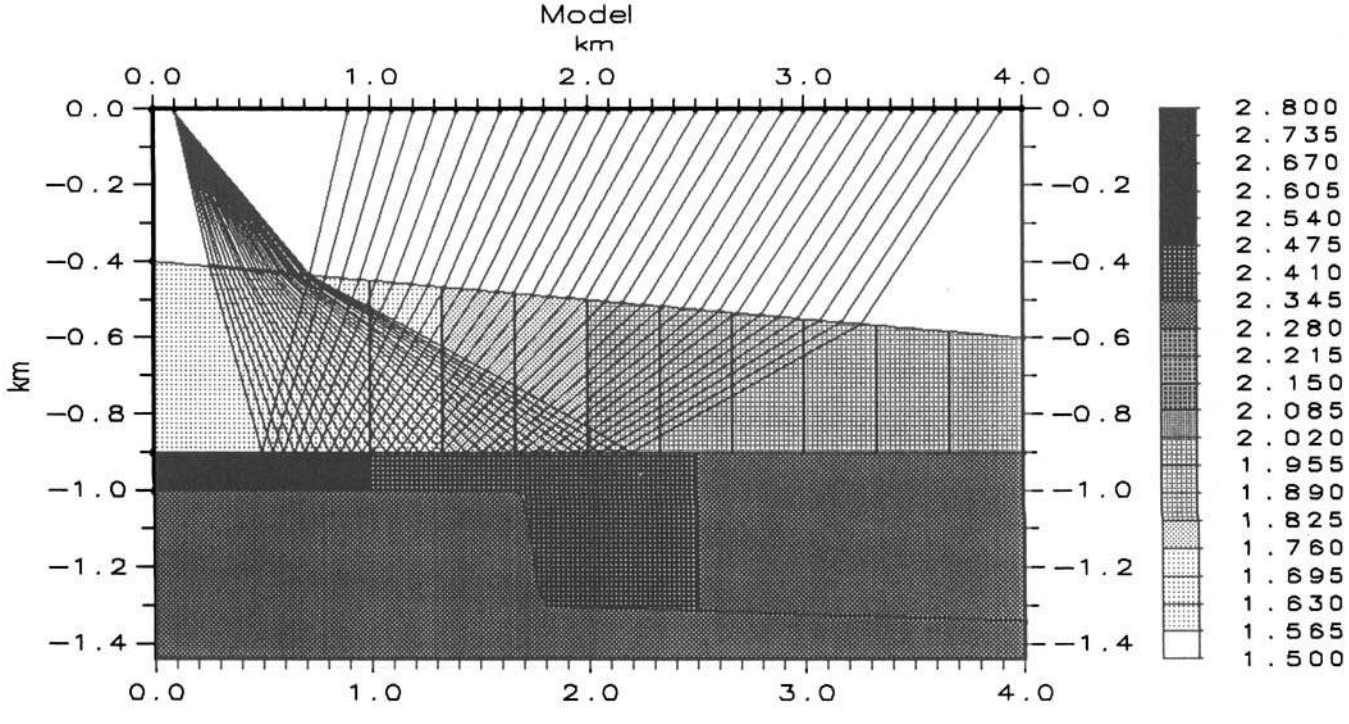

Figure 21. Reflected ray paths in the model of Fig. 19.

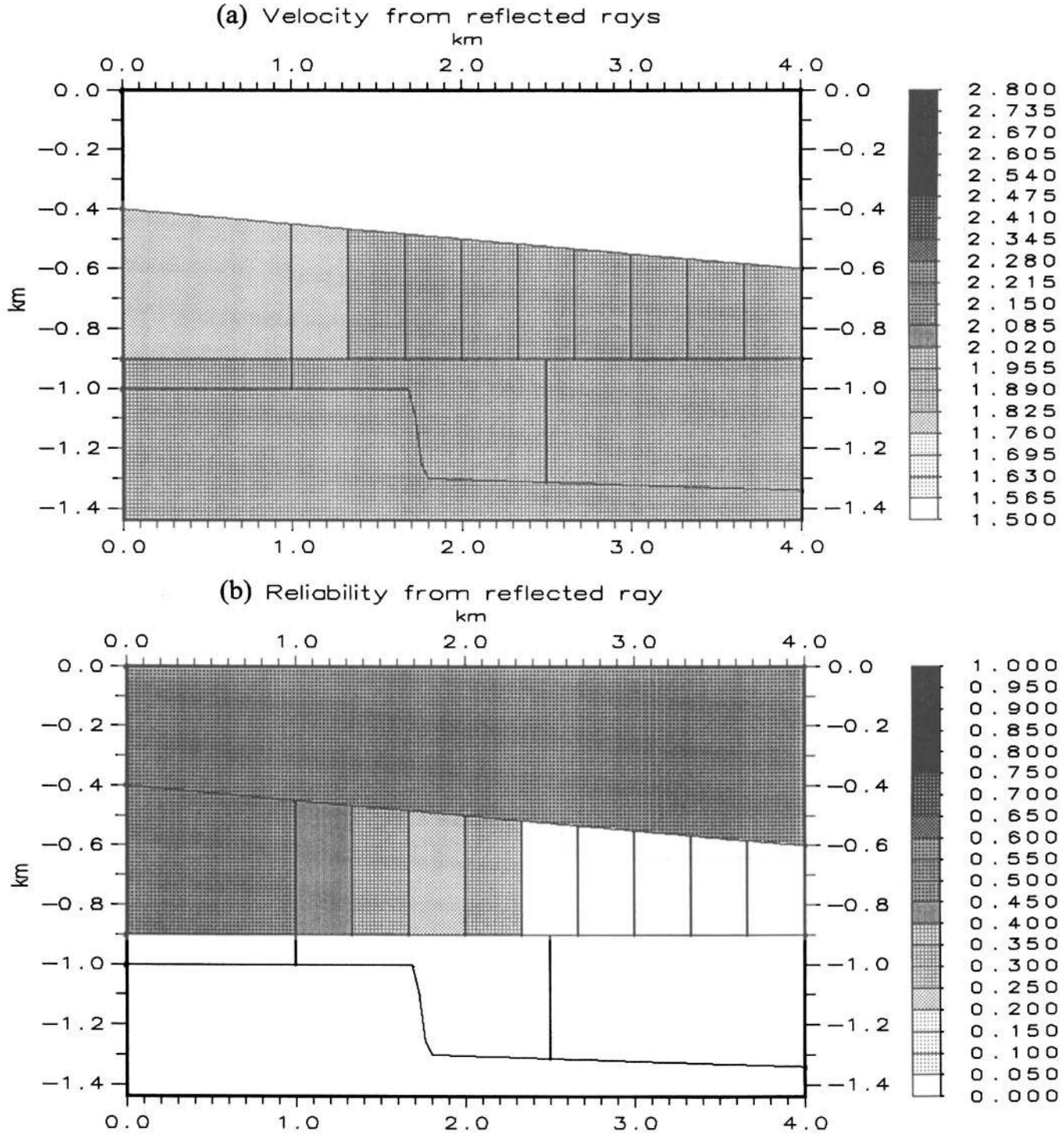

Figure 22. Estimated velocity (a) and reliability (b) of the model in Fig. 19, using reflected waves.

particularly useful in 3-D models, where the total pixel number can be dramatically reduced.

Fermat's principle of minimum time allows one to trace the ray paths not only of reflected and transmitted P and S waves, but also of diffracted, refracted and converted ones. Refracted and diffracted waves can play a significant role in the traveltime inversion, since their ray paths are quite different from those of reflected waves; therefore, they often carry new information, i.e. additional rows in the tomographic matrix that are linearly independent with respect to those of the reflected waves.

A spin-off from the proposed method for tracing the ray path of refracted waves is the possibility of computing the critical distance for complex models at any depth, with possible applications to crustal studies.

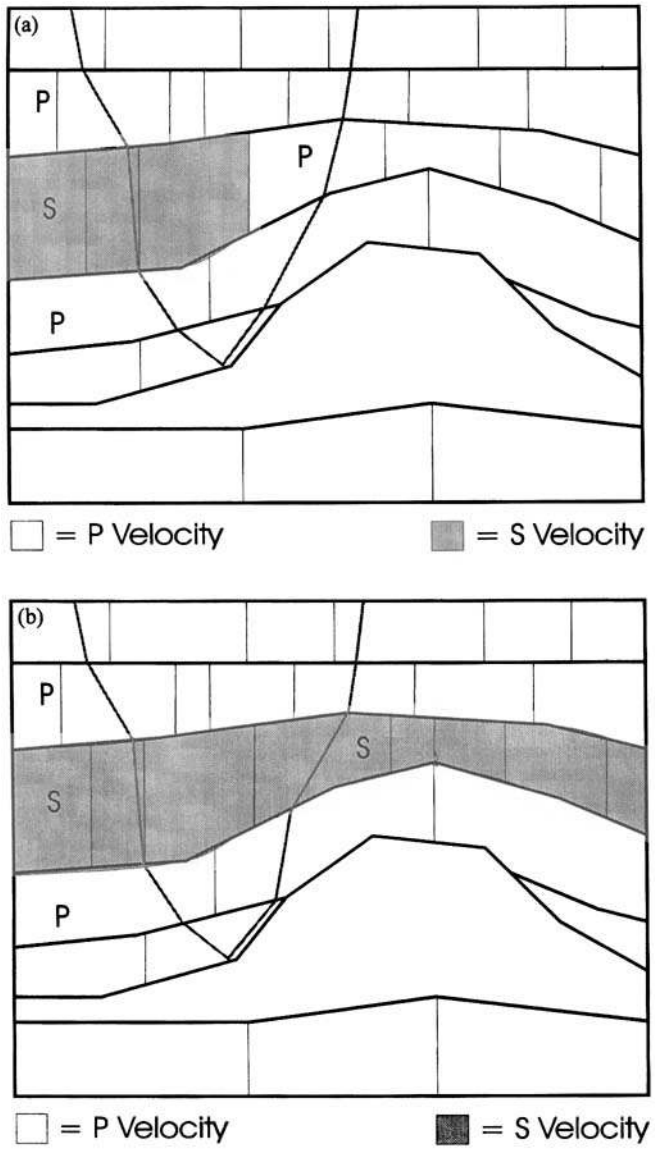

Figure 23. Converted waves can be simulated using *P* or *S* velocity in the appropriate ray segments.

ACKNOWLEDGMENTS

I would like to thank Peter Guidotti for reading the manuscript, and the two anonymous referees for their important remarks and constructive criticism.

REFERENCES

Aki, K. & Richards, P.G., 1980. *Quantitative Seismology, Theory and Methods,* W.H. Freeman, San Francisco.

Al-Chalabi, M., 1974. An analysis of stacking, rms, average and interval velocity over a horizontally layered ground, *Geophys. Prospect.,* **22,** 458–475.

Al-Chalabi, M., 1994. Seismic velocities—a critique, *First Break,* **12,** 589–596.

Asakawa, E. & Kanawaka, T., 1993. Seismic ray tracing using linear traveltime interpolation, *Geophys. Prospect.,* **41,** 99–111.

Backus, G.E. & Gilbert, J.F., 1967. Numerical applications of a formalism for geophysical inverse problems, *Geophys. J. R. astr. Soc.,* **13,** 247–276.

Bamford, D., 1976. MOZAIC time-term analysis, *Geophys. J. R. astr. Soc.,* **44,** 433–466.

Boehm, G., Camerlenghi, A., Lodolo, E. & Vesnaver, A., 1995. Tomographic analysis and geological context of a bottom simulating reflector on the South Shetland Margin (Antarctic Peninsula), *Boll. Geof. Teor. Appl.,* **37,** 3–23.

Boehm, G., Crise, A. & Vesnaver, A., 1996a. Traveltime inversion of marine seismic data for ocean sound speed reconstruction, in *Full Inversion Methods in Ocean and Seismo-acoustics,* pp. 291–296, eds Diachok, O. *et al.,* Kluwer, Boston.

Boehm, G., Carcione, J. & Vesnaver, A., 1996b. Reflection tomography versus stacking velocity analysis, *J. appl. Geophys,* in press.

Carrion, P., 1991. Dual tomography for imaging complex structures, *Geophysics,* **56,** 1395–1404.

Carrion, P., Boehm, G., Marchetti, A., Pettenati, F. & Vesnaver, A., 1993a. Reconstruction of lateral gradients from reflection tomography, *J. explor. Seism.,* **2,** 55–67.

Carrion, P., Marchetti, A., Boehm, G., Pettenati, F. & Vesnaver, A., 1993b. Tomographic processing of Antarctica's data, *First Break,* **11,** 295–301.

Carrion, P., Vesnaver, A., Boehm, G. & Pettenati, F., 1993c. Aperture compensation tomography, *Geophys. Prospect.,* **41,** 367–380.

Cerveny, V., 1987. Ray tracing algorithms in three-dimensional laterally varying layered structures, in *Seismic Tomography with Applications in Global Seismology and Exploration Geophysics,* pp. 99–133, ed. Nolet, G., Reidel, Dordrecht.

Claerbout, J.F., 1976. *Fundamentals of Geophysical Data Processing with Applications to Petroleum Prospecting,* McGraw-Hill, New York.

Dix, C.H., 1955. Seismic velocities from surface measurements, *Geophysics,* **20,** 68–86.

Fisher, R. & Lees, J.M., 1993. Shortest path ray tracing with sparse graphs, *Geophysics,* **58,** 987–996.

Golub, G.H. & Van Loan, C.F., 1983. *Matrix Computations,* North Oxford Academic, Oxford.

Hubral, P. & Krey, T., 1980. *Interval Velocities from Seismic Reflection Time Measurement,* SEG, Tulsa.

Julian, B.R. & Gubbins, D., 1977. Three-dimensional seismic ray tracing, *J. geophys. Res.,* **43,** 95–114.

Kaczmarz, S., 1937. Angenaeherte Aufloesung von Systemen linearer Gleichungen. *Bull. Acad. Polon. Sci. Lett.* A, **35,** 355–357.

Levenberg, K., 1944. A method for the solution of certain non-linear problems in least squares, *Q. appl. Math.,* **2,** 164–168.

Lines, L.R. & Treitel, S., 1984. Tutorial: a review of least-squares inversion and its application to geophysical problems, *Geophys. Prospect.,* **32,** 159–186.

Marquardt, D.W., 1963. An algorithm for least squares estimation of non-linear parameters, *J. Soc. industrial and applied Mathematics,* **11,** 431–441.

Moser, T.J., 1989. Efficient seismic ray tracing using graph theory, *59th Ann. Int. Mtg, Soc. Expl. Geophys., Expanded Abstracts,* 1106–1108.

Moser, T.J., 1991. Shortest path calculation of seismic rays, *Geophysics,* **56,** 59–67.

Neri, A., Carrion, P., Jacovitti, G. & Vesnaver, A., 1993. Tomographic reconstruction from incomplete data set with deterministic and stochastic constraints, *Expanded Abstracts of SPIE Meeting,* in press.

Nolet, G., 1987. *Seismic Tomography with Applications to Global Seismology and Exploration Geophysics,* Reidel, Dordrecht.

Pereyra, V., 1992. Two point ray tracing in general 3-D media, *Geophys. Prospect.,* **40,** 267–287.

Phillips, W.S. & Fehler, M.C., 1991. Traveltime tomography: a comparison of popular methods, *Geophysics,* **56,** 1639–1649.

Press, W., Flannery, B., Teukolsky, S. & Vetterling, W., 1989. *Numerical Recipes,* Cambridge University Press, Cambridge.

Saito, H., 1989. Traveltimes and ray paths of first arrival seismic waves, *59th Ann. Int. Mtg, Soc. Expl. Geophys., Expanded Abstracts,* 244–247.

Shah, P.M., 1973. Use of wavefront curvature to relate seismic data with subsurface parameters. *Geophysics,* **38,** 812–825.
Taner, M.T. & Koehler, F., 1969. Velocity spectra—digital computer derivation and applications of velocity functions, *Geophysics,* **34,** 859–881.
van der Sluis, A. & van der Vorst, H.A., 1987. Numerical solution of large, sparse linear algebraic systems arising from tomographic problems, in *Seismic Tomography with Applications in Global Seismology and Exploration Geophysics,* pp. 49–83, ed. Nolet, G., Reidel, Dordrecht.
Vasco, D.W., 1991. Bounding seismic velocities using a tomographic method, *Geophysics,* **56,** 472–482.
Vesnaver, A. & Boehm, G., 1995. The sampling problem in seismic tomography, *58th EAEG Mtg, Expanded Abstracts,* P131, Zeist.
Vidale, J., 1988. Finite difference calculation of traveltimes, *Bull. seism. Soc. Am.,* **78,** 2062–2076.
Vidale, J., 1990. Finite-difference calculation of traveltimes in three dimensions, *Geophysics,* **55,** 521–526.
Virieux, J. & Farra, V., 1991. Ray tracing in 3-D complex isotropic media: an analysis of the problem, *Geophysics,* **56,** 2057–2069.
Yilmaz, O., 1987. *Seismic Data Processing,* SEG, Tulsa.
Zelt, C.A. & Schmidt, R.B., 1992. Seismic traveltime inversion for 2-D crustal velocity structure, *Geophys. J. Int.,* **108,** 16–34.

APPENDIX A: SINGULAR VALUES AND THE DAMPING FACTOR

Matrix $\mathbf{A}$ can be decomposed as follows:

$$\mathbf{A} = \mathbf{U}\mathbf{W}\mathbf{V}^{\mathrm{T}} \ldots, \tag{A1}$$

where

$$\mathbf{U}^{\mathrm{T}}\mathbf{U} = \mathbf{I}, \qquad \mathbf{V}\mathbf{V}^{\mathrm{T}} = \mathbf{V}^{\mathrm{T}}\mathbf{V} = \mathbf{I}. \tag{A2}$$

The solution $\underline{\mathbf{u}}$ of the damped least-squares inversion is given by

$$\underline{\mathbf{u}} = (\mathbf{A}^{\mathrm{T}}\mathbf{A})^{-1}\mathbf{A}^{\mathrm{T}}\mathbf{t}, \tag{A3}$$

where $\mathbf{t}$ is a vector of traveltimes.

Inserting eqs (1) and (A1) into eq. (A3) and using the properties (A2) gives

$$\underline{\mathbf{u}} = \mathbf{R}\mathbf{u}, \tag{A4}$$

where $\mathbf{u}$ is the 'true' velocity distribution and the resolution matrix $\mathbf{R}$ is

$$\begin{aligned}\mathbf{R} &= (\mathbf{A}^{\mathrm{T}}\mathbf{A} + \lambda\mathbf{I})^{-1}\mathbf{A}^{\mathrm{T}}\mathbf{A} \\ &= (\mathbf{V}\mathbf{W}^{\mathrm{T}}\mathbf{U}^{\mathrm{T}}\mathbf{U}\mathbf{W}\mathbf{V}^{\mathrm{T}} + \lambda\mathbf{I})^{-1}\mathbf{V}\mathbf{W}^{\mathrm{T}}\mathbf{U}^{\mathrm{T}}\mathbf{U}\mathbf{W}\mathbf{V}^{\mathrm{T}} \\ &= \mathbf{I}[\mathbf{W}^2(\mathbf{W}^2 + \lambda\mathbf{I})^{-1}]\mathbf{I}^{\mathrm{T}},\end{aligned} \tag{A5}$$

where $\mathbf{W}^2 = \mathbf{W}^{\mathrm{T}}\mathbf{W}$ is a diagonal matrix. The last expression can be viewed as a singular value decomposition of matrix $\mathbf{R}$, whose singular values r_i are

$$r_i = a_i^2/(a_i^2 + \lambda), \tag{A6}$$

where a_i are the singular values of the tomographic matrix $\mathbf{A}$. A similar result was presented by Lines & Treitel (1984) and by van der Sluis & van der Vorst (1987).

APPENDIX B: INTERPOLATION BY A RATIONAL FUNCTION

An efficient way to build a rational function for a stable and accurate interpolation is described by Press *et al.* (1989). Let us consider, for example, a fourth-order function, interpolating the points (x_0, t_0), (x_1, t_1), (x_2, t_2) and (x_3, t_3). It is necessary to define some working variables:

$$R_1 = t_0, \qquad R_2 = t_1, \qquad R_3 = t_2, \qquad R_4 = t_3; \tag{B1}$$

and, using the recursion

$$\begin{aligned}&R_{i(i+1)\ldots(i+m)} \\ &\quad = R_{(i+1)\ldots(i+m)} \\ &\qquad + \frac{R_{(i+1)\ldots(i+m)} - R_{i\ldots(i+m-1)}}{\left(\dfrac{x - x_i}{x - x_{i+m}}\right)\left(1 - \dfrac{R_{(i+1)\ldots(i+m)} - R_{i\ldots(i+m-1)}}{R_{(i+1)\ldots(i+m)} - R_{(i+1)\ldots(i+m-1)}}\right) - 1},\end{aligned} \tag{B2}$$

we obtain the desired rational function $R_{1234}(x)$, according to the following tree:

$$\begin{array}{ccccc} R_1 & & & & \\ & R_{12} & & & \\ R_2 & & R_{123} & & \\ & R_{23} & & R_{1234} & \\ R_3 & & R_{234} & & \\ & R_{34} & & & \\ R_4 & & & & \end{array} \tag{B3}$$

It is interesting to note that, if a fourth-order function is not sufficiently accurate, all the R coefficients just computed can be reused to build a new fifth- or higher-order rational function.